

Al₂O₃-CaO macroporous ceramics containing hydrocalumite-like phases

O.H., Borges ^{(a)*}; T., Santos Jr ^(a); V. R., Salvini ^(b); V.C., Pandolfelli ^(a)

^(a) Federal University of São Carlos, Graduate Program in Materials Science and Engineering.

^(b) São Paulo State Technological College (FATEC), Rua Jordão Borghetti 480,
Sertãozinho, SP, 14160-050, Brazil

*Corresponding author at: +55-16-33518253; fax: +55-16-33615404.
E-mail: otavio.borges@dema.ufscar.br

Abstract

A mechanism to explain the lower onset strengthening temperature induced by CaCO₃ in alumina-based macroporous ceramics is proposed, which relies on hydrocalumite-like phase formation during processing. Close to 600 °C, such phases are decomposed to lime and mayenite (12CaO·7Al₂O₃), where the latter, due to its intrinsic nanoporosity and high thermal reactivity, generates bonds between the ceramic particles at ~700°C, resulting in microstructure strengthening. Based on this premise, the authors concluded that other Ca²⁺ sources could act similarly. Indeed, compositions containing Ca(OH)₂ or CaO showed the same effect on the onset strengthening temperature, which reinforces the proposed mechanism. The results attained indicated that macroporous insulators could be thermally treated at lower temperatures, just to acquire enough mechanical strength for installation, finishing *in-situ* their firing process. Besides that, lower sintering temperatures could be used to produce macroporous ceramics that would be applied in low thermal demand environments, e.g. aluminum industries.

Keywords: macroporous insulators, hydrocalumite, mayenite, sintering.

DOI: 10.1016/j.ceramint.2019.11.046



1 Introduction

The development of new technologies has always been closely linked to energy consumption. This trend and the fact that the world main power supplies are non-renewable and highly polluting, has resulted in increasing concern about the energy issue [1–3]. According to the International Energy Agency (IEA), the industrial sector plays a key role in energy demand, accounting for 37 % of the total amount spent in 2017 [4]. In addition, special attention should be given to industrial high temperature processes (above 1300 °C), as they are responsible for one-third of the industrial power demand [5]. In this case, much of the energy consumed is used to heat, adjust or maintain the temperature of different equipment, such as furnaces and boilers. Thus, thermal insulators, which reduce heat losses, can help these processes by lowering the energy costs and helping the environment [1,4,5].

Various refractory thermal insulators were developed for this purpose. Among them, those of greater commercial importance are currently comprised by ceramic fibers [6,7]. Even though these materials are easily available and present low thermal conductivity at room temperature, they have a short lifecycle due to the high surface area of fibers and the presence of SiO₂-containing binders, which might undergo densification in service. Moreover, these insulators can be highly toxic when inhaled and some compositions are classified as carcinogenic by the International Agency for Research on Cancer (IARC) [8,9].

Therefore, the search for novel non-toxic thermal insulators able to withstand high temperatures with a longer lifecycle is of great scientific and technological interest. One of the options that emerges as a promising alternative is the macroporous refractories [6]. By definition, they comprise a refractory matrix containing pores with a diameter greater

than 50 nm, which are present in a volumetric fraction above 40% [10,11]. This microstructure is able to halt both the heat transference by phonons, due to the discontinuities in the solid crystalline lattice (pores), and by radiation, as pores in the range of 0.5 μm to 3 μm can interact with electromagnetic waves in the infrared spectra, spreading them [12].

Thus, some macroporous refractories exhibit similar values of effective thermal conductivity when compared to fibrous blankets and bricks, having the added advantage of being non-toxic and presenting a superior lifecycle, as they do not densify in service, when previously fired [6,13]. However, there are some challenges to overcome if macroporous refractories are to be more widely used to replace fiber-based insulators. For example, this material needs to be pre-sintered at high temperatures in order to achieve suitable mechanical strength, even if its application is for lower thermal demand environments.

Recently, it was reported that by using CaCO_3 in alumina-based dense refractories, besides inducing hibonite formation ($\text{CaO}\cdot 6\text{Al}_2\text{O}_3$, also referred to as CA_6) that helps to reduce materials' thermal conductivity, and it is also capable of decreasing the strengthening onset temperature [14]. Investigating this effect, Luz *et al.* [14] reported the elastic modulus increase of dense alumina-based refractory castables as a function of temperature, by changing the CaCO_3 - CAC ratio (see Figure 1). However, the mechanism by which this effect takes place has not yet been explained. It is worth highlighting that Lin and Shen [15] described an effect called Sintering-Coarsening-Coalescence (SCC) on CaCO_3 particles exposed to temperatures close to 400 $^\circ\text{C}$, but the reasons why refractories containing CaCO_3 and Al_2O_3 showed E increase at lower temperatures remain unclarified.

Figure 1

Additionally, the Layered Double Hydroxide (LDH) phase formation in refractories processed in the presence of water has been studied with promising results, so far [16]. LDHs with hydrocalumite structure can be generated in systems containing Al^{3+} and Ca^{2+} ions in aqueous media [17], which is comprised by alternated stacks of calcium and aluminum hydroxide layers, with their interlamellar spaces filled in with charged species [17]. Hydrocalumite-like phases present the following chemical formula $[\text{Ca}_2\text{Al}(\text{OH})_6]^+\text{X}^- \cdot m\text{H}_2\text{O}$, where X is the anion located in the interlamellar space counterbalancing the positive charges, *e.g.* OH^- , CO_3^{2-} and Cl^- [18,19]. This hydrate phase decomposes close to 600 °C, resulting in lime (CaO) and mayenite ($12\text{CaO} \cdot 7\text{Al}_2\text{O}_3$ or C_{12}A_7) [17].

Moreover, it is known that mayenite has intrinsic nanometric porosity resulted by the nanosized cages present in its microstructure, which are partially filled by weakly bounded O^{2-} [20,21]. This feature classifies mayenite as an anti-zeolite phase. Recent studies pointed out that mayenite, besides releasing peroxide ions from 350 °C to 650 °C, reducing the number of filled cages, undergoes phase transition close to 650 °C, giving rise to a phase in which the lattice parameter increases more rapidly with the temperature [20,22].

These data might induce the correlation between the effect reported by Luz *et al.* [14] for dense refractories with those related to hydrocalumite-like phase formation at the interface among the ceramic particles, which results in CaO and C_{12}A_7 during thermal treatment. In addition, this hypothesis can predict that other Ca^{2+} sources will also be able

to generate such an effect, anticipating the onset strengthening temperature, as long as they form hydrocalumite-like phases during the processing.

In order to analyze this hypothesis, the hydrocalumite-like phase formation during the macroporous alumina-based insulator processing, containing both CaCO_3 and Ca(OH)_2 , was evaluated. Following that, the elastic modulus *versus* temperature profile ($E_{in\ situ}$) for compositions containing distinct Ca^{2+} sources was carried out.

2 Materials and methods

2.1 Materials

To investigate the LDH formation for compositions containing CaCO_3 and Ca(OH)_2 , samples with hydrocalumite stoichiometric quantities of Al^{3+} and Ca^{2+} were produced in order to maximize their formation, and thus enable their detection. One composition presented CaCO_3 as Ca^{2+} precursor (RHI Magnesita, Brazil, $D_{90} = 12.64\ \mu\text{m}$, $D_{50} = 7.38\ \mu\text{m}$, $D_{10} = 1.49\ \mu\text{m}$), whereas the other contained Ca(OH)_2 (Synth, Brazil, 99.9% purity, $D_{90} = 11.00\ \mu\text{m}$, $D_{50} = 5.66\ \mu\text{m}$, $D_{10} = 2.76\ \mu\text{m}$). In both, alumina CL 370 (Almatis, Germany, $D_{50} = 2.5\ \mu\text{m}$) was used as an Al^{3+} source. Ceramic powders were added to a beaker with distilled water to result in a suspension with 20 wt% of solids and kept under stirring for 30 minutes at room temperature. Finally, the samples were dried firstly at $50\ ^\circ\text{C}$ for 24 h and then at $110\ ^\circ\text{C}$ for another 24 h, generating a white powder.

Besides these samples, specially prepared to identify the hydrocalumite-like phase formation in the systems tested, formulations of macroporous ceramics were produced to investigate the effect of distinct Ca^{2+} sources on the earlier Young modulus increase and other properties. These compositions comprised a liquid foam containing alumina and different binders and Ca^{2+} sources. The foam formulation and the additives evaluated in

this study are presented in Table 1 and Table 2, respectively. It should be emphasized that the equivalent percentage of CaO was kept constant (1.7 wt%) in order to generate 20 wt% of CA₆ in the samples under thermodynamic equilibrium.

Macroporous ceramics were prepared by direct foaming technique [23], by incorporating a previously prepared liquid foam into an alumina-based suspension. Alumina CL370 and CT3000SG (Almatis, Germany) were used in the appropriate proportion to obtain maximum packaging according to the Andreasen packing model ($q = 0.37$). Alumina suspensions were prepared with distilled water, adding Castament® FS60 (BASF, Germany) and a non-ionic surfactant based on alkylpolyethylene glycol ether (Lutensol® AT 50 Pulver, BASF, Germany) as dispersing agents.

The liquid foam was prepared with a commercial liquid surfactant based on 1,2-benzisothiazol-3(2H)-one (Vinapor GYP 2680, BASF, Germany) and the thickening additive Hydroxyethyl Cellulose (Cellulose® 100 CG FF, Dow, USA). Hydratable alumina (Alphabond 300, Almatis, Germany) or calcium aluminate cement (CAC, Secar 71, Imerys Aluminates, France) were used as binders. Besides CAC, CaCO₃, Ca(OH)₂ and CaO (obtained from CaCO₃ calcination at 900 °C for 4 hours and presenting D₉₀ = 7.97 μm, D₅₀ = 3.24 μm, D₁₀ = 1.36 μm) were used as Ca²⁺ sources.

Table 1: Alumina ceramic foam composition.

	Components	wt%
Al₂O₃ Suspension	CL370	76.06
	CT3000SG	5.72
	Castament® FS60	0.09
	Lutensol AT50	0.1
	Water	15.79
Foam	Vinapor GYP 2680	3.4680
	Hydroxietil Cellulose	0.0056

Table 2: Binders and lime sources used for each ceramic foam formulation.

		Additive (wt%)				
		Secar 71	AlphaBond 300	CaCO ₃	Ca(OH) ₂	CaO
Formulation	REF	-	1.00	-	-	-
	5 % CAC	5.00	-	-	-	-
	0.53 % CaCO ₃ +CAC	4.00	-	0.53	-	-
	2.04 % CaCO ₃ +CAC	1.00	-	2.04	-	-
	1.55 % Ca(OH) ₂ +CAC	1.00	-	-	1.55	-
	1.42 % Lime	-	-	-	-	1.42

For processing the samples, initially FS60 was dissolved in water, followed by adding the aluminas and Lutensol AT50. Then, the system was maintained under intense mechanical stirring for ~ 30 minutes. After that, the additives (Table 2) were incorporated to each composition, except for CAC and calcined CaO ones, which, due to their faster hydration kinetics, had to be added at the last processing step. A liquid foam was produced by mechanical stirring Vinapor GYP 2680 and Cellulose® 100 CG FF. After preparing the foam, it was mixed with the alumina suspension under minimal stirring (30 rpm). Finally, the liquid foam containing ceramic particles was cast into cylinder (50 mm x 50 mm) and bar (150 mm x 25 mm x 25 mm) molds. Compositions REF and 1.42 % Lime were cured at 50 °C for 24 h and dried at 110 °C for another 24 h. The other compositions containing CAC were cured in a climatic chamber at 50 °C and humidity of 80 % for 24 hours, then dried at 110 °C for 24 h.

2.2 Methods

The samples specially prepared to enable hydrocalumite-like phase detection were analyzed by Fourier transform infrared diffraction spectroscopy (DRIFT) using Equinox 55 equipment (Brüker, Karlsruhe, Germany). The samples were scanned with wavelengths in the range between 400 nm and 4000 nm with a resolution of 0.4 nm and

32 scans per wavelength. In addition, DRIFT scans were carried out for the raw materials used to produce the evaluated suspensions, in order to compare their transmittance spectra.

X-ray diffraction (XRD) was performed to investigate hydrocalumite-like phase formation. Due to difficulties of identifying these phases by XRD of green samples, they were calcined at 700 °C for 2 hours, allowing the decomposition of the likely present hydrocalumite. Therefore, the detection of mayenite in these samples (which in systems containing CaO and Al₂O₃ is expected to be formed close to 1300 °C [24]) would indicate the presence of hydrocalumite-like phases in the initial systems. XRD analyses were carried out in Geiger-Flex diffractometer (Rigaku, Tokyo, Japan) in the 4 ° to 90 ° range, with 0.02 ° step and using copper K α radiation and nickel filter. The results were compared to diffraction patterns from the International Diffraction Data Center (ICDD) database.

The macroporous ceramic foams were characterized by their elastic modulus *versus* temperature profiles (*E_{in situ}*) in Scanelastic 02 (ATCP Physics Engineering, Brazil), using the resonance frequency scanning method according to ASTM E1875 [25]. Elastic moduli were measured every 5 minutes up to 1400 °C and back to room temperature, with a heating and cooling rate of 2 °C.min⁻¹. Additionally, cold crushing strength (ASTM C133-97 [26]) and linear shrinkage were measured for the 2.04 % CaCO₃+CAC composition in their green condition (after drying at 110 °C for 24 h) and after firing at 400 °C, 600 °C, 800 °C and 1000 °C for 5 hours.

Mineralogical analysis of macroporous ceramic samples were carried out to evaluate whether the predicted CA₆ content would actually be achieved after firing at

1600 °C for 5 hours. Thus, fired samples were ground and the powder was analyzed by X-ray diffraction at the previously described conditions. The obtained patterns underwent Rietveld refinement using Topas software (Bruker, Massachusetts, USA) and ensuring Goodness of Fit (GOF) < 1.5 and weighted profile R-factor (RWP) < 15 %.

3 Results and Discussion

3.1 Diffuse reflectance infrared Fourier transform spectroscopy (DRIFT)

Samples containing alumina and CaCO₃ or Ca(OH)₂, named CL370+CaCO₃ and CL370+Ca(OH)₂, respectively, were characterized by DRIFT. Figure 2 shows the spectra for each sample, their precursors and that of hydrocalumite, as reported by Tian and Guo in [17]. It can be observed that CL370+CaCO₃ and CL370+Ca(OH)₂ presented almost all characteristic bands of hydrocalumite. In this regard, absorption band at 3640 cm⁻¹ represents the stretching vibrations of lattice water together with surface-absorbed H₂O. The radiation absorption close to 3485 cm⁻¹ is related to OH⁻ stretching vibrations in the portlandite-like layers of hydrocalumite, whereas in the range of 1640 cm⁻¹ it is assigned to the H-O-H bending vibrations of the interlayer water. Infrared waves close to 1445 cm⁻¹ induce vibrations for the adsorbed CO₂ bonds.

Figure 2

Moreover, the absorption bands at 789 cm⁻¹, 533 cm⁻¹ and 428 cm⁻¹ for the hydrocalumite are related to stretching vibrations of OH- groups linked to metal elements [17,27]. Therefore, despite not showing some absorption bands in the range of 789 cm⁻¹ and 428 cm⁻¹, the DRIFT results pointed out that phases with hydrocalumite structure were formed in both CL370+CaCO₃ and CL370+Ca(OH)₂ compositions. However, the

other bands presented in these samples, but not in hydrocalumite, highlighted that not all reactants were consumed to form the LDH phase. Additionally, it is expected that adding calcined CaO will also result in hydrocalumite formation, as it reacts with water generating Ca(OH)₂ [28].

The presence of hydrocalumite-like phases in the characterized samples was also confirmed by the XRD, as discussed as follows.

3.2 X-ray diffraction (XRD)

Figure 3 shows X-ray profiles for samples of CL370+CaCO₃ and CL370+Ca(OH)₂ after thermal treatment at 700 °C for 2 h. The diffraction peaks show the presence of corundum, lime and mayenite in both compositions highlighted above.

Mayenite in the CaO-Al₂O₃ system is expected above 1300 °C, therefore its presence at 700 °C reinforces the hypothesis of hydrocalumite formation, as this phase decomposes close to 600 °C resulting in CaO and C₁₂A₇ [17]. Additionally, it can be observed that not all initial materials reacted to form hydrocalumite-like phases. These results are in agreement with those obtained by DRIFT and suggest that hydrocalumite-like phases could be formed during the processing of macroporous alumina-based refractories containing CaCO₃, Ca(OH)₂ or CaO as Ca²⁺ sources and produced by direct foaming.

Figure 3

3.3 In situ elastic modulus of compositions with different CaCO₃/CAC ratios

Elastic modulus (E) evaluation with temperature was carried out for green samples of REF, 5 % CAC, 0.53 % CaCO₃+CAC and 2.04 % CaCO₃+CAC compositions in order

to analyze the effect of CaCO_3 on the initial E increase temperature, as previously reported by Luz *et al.* [14] for dense refractory castables. The results can be seen in Figure 4.

All CAC-containing compositions showed an E drop in the temperature range between 100 °C and 450 °C, which is related to the decomposition of hydrated phases [29]. For the REF sample, two E drop temperatures could be seen, one close to 100 °C and the other about 200 °C. The first occurs due to the evaporation of free water, whereas the second is related to pseudoboehmite decomposition, an usual phase for hydratable alumina-based refractories [30].

Figure 4

All compositions in Figure 4 present similar initial E values. Nevertheless, after thermal treatment, it can be seen that the REF one showed the highest one at the end of the cycle, which can be explained by its high linear shrinkage (55 % above the average of the other compositions), which resulted in lower porosity. In fact, after firing REF at 1600 °C for 5 h, it showed 25 % less porosity than the Ca^{2+} containing compositions. For CaCO_3 -containing samples, the higher carbonate content resulted in superior E at the end of the measurements. This behavior could be assigned to morphological differences in the *in situ* formed CA_6 . When interacting with small alumina particles, CaCO_3 favors the generation of acicular hibonite [24], which provides additional strengthening.

Compositions 5 % CAC and REF presented similar temperatures of the initial E increase (950 °C), which is associated to the beginning of reactive alumina sintering. Thus, it can be concluded that neither CAC nor HA resulted in a significant change in

lowering the strengthening temperature. On the other hand, for CaCO_3 -containing compositions, a correlation was observed between the CaCO_3 amount and the initial temperature of E increase (780 °C and 700 °C for 0.53 % CaCO_3 +CAC and 2.04 % CaCO_3 +CAC, respectively). These results agree with the ones reported by Luz *et al.* [14]. It is worth observing that for CaCO_3 -based compositions, the expected decrease in the E values during carbonate decomposition (carried out close to 800 °C) was not observed. This phenomenon, which was also observed for dense refractories [14], could be attributed to the high E increase at this temperature, which overlaps the decrease expected during the CaCO_3 decomposition.

Additionally, the correlation between the lower onset strengthening temperature and the presence of hydrocalumite-like phases stands out because, unlike HA and CAC, CaCO_3 is able to form these LDHs during the refractory processing [31–34].

3.4 *Crushing strength and linear shrinkage versus temperature*

Moving on to understanding how hydrocalumite-like phases affect the strengthening onset temperature, cold crushing strength and linear shrinkage after thermal treatment were carried out for the 2.04 % CaCO_3 +CAC samples. This composition was selected because of its higher likelihood of hydrocalumite generation. The samples were fired at 400 °C, 600 °C, 800 °C and 1000 °C for 5 hours with a heating rate of 2 °C.min⁻¹ and the results are shown in Figure 5.

Figure 5

Compared to the green condition, thermal treatment at 400 °C and 600 °C for 5 h did not present significant changes either in crushing strength or in linear shrinkage. On

the other hand, samples fired at 800 °C and 1000 °C showed a significant cold crushing strength increase (close to 640 % and 1080 %, respectively) without relevant linear shrinkage. These low values of shrinkage indicate that the strengthening mechanism carried out in the range of 600 °C and 1000 °C did not involve the classic densification process.

Thus, this work proposes that the observed strengthening mechanism takes place due to hydrocalumite-like phases formed on the particles' surface during the processing stage. As previously mentioned, this LDH phase decomposes around 600 °C resulting in lime and mayenite [17]. The mayenite formed contains intrinsic nanoporosity and undergoes a phase transition at 650 °C, which makes it even more reactive [20,22]. Therefore, it is expected that highly reactive mayenite located in some particles' interfaces could react by linking them. As a result, an increase of mechanical strength without shrinkage can be observed before sintering takes place, whereby the latter is expected to occur above 950 °C.

Looking carefully at Figure 4, it is worth observing that there was no high increase in the E value around 950 °C for CaCO₃-containing compositions, but a constant and smooth increment was noticed. Although further investigations are required, this behavior could be assigned to the particles' links induced by highly reactive mayenite, which lead to mechanical strength values close to those driven by primary chemical bonding after sintering.

3.5 *In situ elastic modulus of different Ca²⁺ sources*

After evaluating the mechanical strengthening induced by CaCO₃ at lower temperatures, the proposed mechanism and the results from DRIFT and DRX (presented in Figure 2 and Figure 3, respectively), were all used to forecast that an analogous effect

should take place by using $\text{Ca}(\text{OH})_2$ and CaO sources, instead of CaCO_3 , as in either cases hydrocalumite-like phases are expected to be formed. To evaluate this prediction, compositions containing calcium hydroxide [1.55 % $\text{Ca}(\text{OH})_2$ +CAC] and calcium oxide (1.42 % Lime) had their *in situ* E values evaluated. The results are presented in Figure 6, which also reports data for compositions 5 % CAC and 2.04 % CaCO_3 +CAC.

Figure 6

Initially, the E decrease in the temperature range between 100 °C and 400 °C was observed for the 1.55 % $\text{Ca}(\text{OH})_2$ +CAC composition. This behavior, similar to that presented by 2.04 % CaCO_3 +CAC, is related to the hydrated CAC phase decomposition and dehydration of $\text{Ca}(\text{OH})_2$, in which the latter is expected at temperatures close to 400 °C [35]. On the other hand, 1.42 % Lime composition showed just one E drop, which can be explained by the absence of CAC and by the CaO hydration during the foam processing, which leads to $\text{Ca}(\text{OH})_2$ formation, as previously mentioned. Therefore, the E drop at ~ 400 °C is caused by $\text{Ca}(\text{OH})_2$ decomposition. It is also worth observing that the 5 % CAC composition presented the lowest mechanical strengthening after firing ($E_{\text{final}} - E_{\text{initial}}$), which is most likely due to the formation of highly asymmetric platelet CA_6 grains induced by using CaCO_3 and $\text{Ca}(\text{OH})_2$ [24].

Analyzing the impact of each Ca^{2+} source on the strengthening, it is clear that CaCO_3 , $\text{Ca}(\text{OH})_2$ and CaO reduced the temperature for initial E increase to 700 °C, whereas for CAC, this temperature was close to 950 °C. This behavior reinforces the connection between the hydrocalumite-like phase formation and the lower strengthening

onset temperature, as CaCO_3 , Ca(OH)_2 and CaO can develop such phases during the refractory foam processing.

The main advantages on this earlier E increase induced by Ca^{2+} sources can be summarized as: (i) macroporous insulators could be thermally treated at lower temperatures, just to acquire enough mechanical strength for transportation and installation, finishing *in situ* their firing process; (ii) lower sintering temperatures can be used to produce macroporous ceramics that would be applied in low thermal demand environments, e.g. aluminum industry. In both situations, the energy input required to manufacture the macroporous material would be reduced.

Another environmental advantage which stands out is the possibility of replacing, at least in part, the amount of CAC by CaCO_3 . Calcium aluminate cement manufacturing typically uses Al(OH)_3 and CaCO_3 as raw materials, which are processed at a high temperature (1550 °C) [36], whereas CaCO_3 is found in nature as lime deposits. Therefore, this replacement would lead to reductions on macroporous refractory carbon footprints.

3.6 Quantitative phase analysis by XRD

As previously pointed out, CA_6 formation could bring benefits to macroporous insulators, e.g. lower thermal conductivity and firing shrinkage. With this in mind, fired samples (1600 °C for 5 hours) of each formulation had their mineralogical composition quantified by Rietveld Analysis of XRD patterns. The raw patterns and quantitative phase content are presented in Figure 7 and Table 3, respectively.

The expected CA_6 amount (20 wt%) was formed after the thermal treatment for all compositions showing that the Ca^{2+} sources tested [CaCO_3 , Ca(OH)_2 , CaO and CAC]

were able to react with alumina at 1600 °C for 5 hours, resulting in hibonite. Thus, the applied conditions were enough to achieve the thermodynamic equilibrium, leading to the formation of a refractory phase, which can result in higher chemical and dimensional stability to the macroporous ceramic.

Figure 7

Table 3: Quantitative phase analysis of fired ceramic foams with distinct Ca^{2+} sources based on the Rietveld refinement of X-ray diffraction patterns.

Formulations	Corindum (%wt)	Hibonite (%wt)
REF	100	0
5 % CAC	80.34	19.66
0.53 % CaCO_3+CAC	78.52	21.48
2.04 % CaCO_3+CAC	79.61	20.39
1.55 % $\text{Ca}(\text{OH})_2$+CAC	80.29	19.71
1.42 % Lime	80.44	19.56

However, despite the use of CaCO_3 , $\text{Ca}(\text{OH})_2$ and CaO providing similar benefits to the elastic modulus and mineralogical composition after firing, each Ca^{2+} source can result in different physical properties for the final material. CA_6 morphology, mechanical strength, thermal conductivity, linear shrinkage and porosity are some of them. A further paper discussing the impact of distinct Ca^{2+} sources on the physical properties of macroporous refractory ceramics is being prepared and will be submitted soon.

4 Conclusions

In this work, the correlation between hydrocalumite-like phase formation during the macroporous ceramic processing and a lower strengthening onset temperature, was

studied. Initially, the generation of such phases was observed in systems containing either CaCO_3 or Ca(OH)_2 . Carbonate-containing compositions had their *in situ* elastic modulus evaluated, showing lower strengthening onset temperature. Aiming to understand this phenomenon, crushing strength and linear shrinkage for the 2.04 % CaCO_3 +CAC composition, fired at distinct temperatures, were measured. From the results obtained, it was observed that the strengthening process indeed started in the 600 °C – 800 °C temperature range, without undergoing densification.

Based on the previous results, a mechanism was proposed: Hydrocalumite-like phases generated on the particles' surface during the processing stage, decompose at 600 °C forming lime and highly reactive mayenite ($12\text{CaO}\cdot 7\text{Al}_2\text{O}_3$). This latter phase, located on some particles' interfaces, could react close to 700 °C linking them and resulting in strengthening without shrinkage. Similar results were also observed for compositions containing either Ca(OH)_2 or CaO , which support the proposed mechanism, as the selected Ca^{2+} sources are able to form hydrocalumite-like phases during the refractory processing.

Therefore, the use of CaCO_3 , Ca(OH)_2 or CaO could result in macroporous refractory ceramics thermally treated at lower temperatures, which can reduce the energy required to manufacture this type of material. Additionally, replacing part of the CAC content by CaCO_3 would lead to lower carbon footprints. Finally, all Ca^{2+} sources tested were able to form the expected CA_6 content after firing at 1600 °C for 5 h and each one of them resulted in different macroporous insulator physical properties, which will be further discussed in a forthcoming paper.

5 Acknowledgments

This study was financed in part by the Coordenação de Aperfeiçoamento de Pessoal de Nível Superior - Brasil (CAPES) - Finance Code 001, the Conselho Nacional de Desenvolvimento Científico e Tecnológico – Brasil (CNPq) – Process 130843/2018-0, and Fundação de Amparo à Pesquisa do Estado de São Paulo – Brasil (FAPESP) – Process 2018/07745-5. Additionally, the authors are thankful to BASF Construction Solutions GmbH, to RHI-Magnesita, to Dr. Roger Gonçalves for the DRIFT's analyses and to FIRE – International Federation for Refractory Research and Education.

6 References

- [1] R.C. Armstrong, C. Wolfram, K.P. De Jong, R. Gross, N.S. Lewis, B. Boardman, A.J. Ragauskas, K. Ehrhardt-Martinez, G. Crabtree, M. V. Ramana, The frontiers of energy, *Nat. Energy*. 1 (2016) 1–8. doi:10.1038/nenergy.2015.20.
- [2] P. Changhyup, M.K. Joe, T. Ahn, A stochastic approach for integrating market and technical uncertainties in economic evaluations of petroleum development, *Pet. Sci.* 6 (2009) 319–326. doi:10.1007/s12182-009-0051-7.
- [3] H. Crane, E. Kinderman, R. Malhotra, *A cubic mile of oil: realities and options for averting the looming global energy crisis*, 1st ed., Oxford: Oxford University Press, 2010.
- [4] IEA, *World Energy Balances*, OECD, 2019. Available at <https://webstore.iea.org/world-energy-balances-2019>.
- [5] G. Schierning, Bring on the heat, *Nat. Energy*. 3 (2018) 92–93. doi:10.1038/s41560-018-0093-4.
- [6] D.O. Vivaldini, A.A.C. Mourão, V.R. Salvini, V.C. Pandolfelli, Review: Fundamentals and materials for the microstructure design of high performance refractory thermal insulating, *Cerâmica*. 60 (2014) 297–309. doi:10.1590/S0366-69132014000200021. (in Portuguese).
- [7] V.R. Salvini, J.A. Rodrigues, W.T. Neto, V.C. Pandolfelli, Designing insulating ceramic foams for high temperature furnace lining, *Refract. Worldforum*. 2 (2017) 1–5.
- [8] U. S. National Toxicology Program, Ceramic fibers (respirable size), *Rep. Carcinog. Carcinog. Profiles*. 12 (2011) 89–90. <http://www.asbestoscounsel.com/reports/ceramic-fibers-respirable-size>.
- [9] D.M. Bernstein, J.M. Riego Sintes, B.K. Ersboell, J. Kunert, Biopersistence of synthetic mineral fibers as a predictor of chronic intraperitoneal injection tumor response in rats, *Inhal. Toxicol.* 13 (2001) 851–875. doi:10.1080/08958370175

2378142.

- [10] P.S. Chen, G.F. Liu, *Porous Materials*, 1^a, Elsevier Ltd, Butterworth-Heinemann, 2014. <http://www.sciencedirect.com/science/article/pii/B9780124077881000010>.
- [11] H. Sawai, L.E. Orgel, *IUPAC Compendium of Chemical Terminology*, IUPAC, Research Triangle Park, NC, NC, 2009. doi:10.1351/goldbook.
- [12] P.I.B.G.B. Pelissari, R.A. Angélico, V.R. Salvini, D.O. Vivaldini, V.C. Pandolfelli, Analysis and modeling of the pore size effect on the thermal conductivity of alumina foams for high temperature applications, *Ceram. Int.* 43 (2017) 13356–13363. doi:10.1016/j.ceramint.2017.07.035.
- [13] V.R. Salvini, A.P. Luz, V.C. Pandolfelli, High temperature Al₂O₃ - CA₆ insulating foamed ceramics: processing and properties, *Interceram - Refract. Man.* 59 (2012) 335–339.
- [14] A.P. Luz, L.B. Consoni, C. Pagliosa, C.G. Aneziris, V.C. Pandolfelli, Sintering effect of calcium carbonate in high-alumina refractory castables, *Ceram. Int.* 44 (2018) 10486–10497. doi:10.1016/j.ceramint.2018.03.066.
- [15] P.W. Lin, P. Shen, Onset sintering-coarsening-coalescence kinetics of calcite powders, *J. Eur. Ceram. Soc.* 33 (2013) 3265–3272. doi:10.1016/j.jeurceramsoc.2013.06.023.
- [16] T. dos Santos, F.G. Pinola, A.P. Luz, C. Pagliosa, V.C. Pandolfelli, Al₂O₃-MgO refractory castables with enhanced explosion resistance due to *in situ* formation of phases with lamellar structure, *Ceram. Int.* 44 (2018) 8048–8056. doi:10.1016/j.ceramint.2018.01.246.
- [17] J. Tian, Q. Guo, Thermal decomposition of hydrocalumite over a temperature range of 400 – 1500 °C and its structure reconstruction in water, *J. Chem.* (2014) 1–8. doi:10.1155/2014/454098.
- [18] U.. Birnin-Yauri, F.. Glasser, Friedel's salt, Ca₂Al(OH)₆(Cl,OH)·2H₂O: its solid solutions and their role in chloride binding, *Cem. Concr. Res.* 28 (1998) 1713–1723. doi:10.1016/S0008-8846(98)00162-8.
- [19] A. Gácsi, B. Kutus, Z. Kónya, Á. Kukovecz, I. Pálinkó, P. Sipos, Estimation of the solubility product of hydrocalumite–hydroxide, a layered double hydroxide with the formula of [Ca₂Al(OH)₆]OH· n H₂O, *J. Phys. Chem. Solids.* 98 (2016) 167–173. doi:10.1016/j.jpcs.2016.07.004.
- [20] A.S. Tolkacheva, S.N. Shkerin, I. V. Korzun, S. V. Plaksin, V.R. Khrustov, D.P. Ordinartsev, Phase transition in mayenite Ca₁₂Al₁₄O₃₃, *Russ. J. Inorg. Chem.* 57 (2012) 1014–1018. doi:10.1134/S0036023612070182.
- [21] S. Matsuishi, K. Hayashi, M. Hirano, I. Tanaka, H. Hosono, Superoxide ion encaged in nanoporous crystal 12CaO·7Al₂O₃ studied by continuous wave and pulsed electron paramagnetic resonance, *J. Phys. Chem. B.* 108 (2004) 18557–18568. doi:10.1021/jp046963s.
- [22] S.N. Shkerin, A.S. Tolkacheva, I. V. Korzun, S. V. Plaksin, E.G. Vovkotrub, E. V. Zabolotskaya, Phase transitions in mayenite, *J. Therm. Anal. Calorim.* 124 (2016) 1209–1216. doi:10.1007/s10973-016-5282-4.

- [23] V.R. Salvini, P.R.O. Lasso, A.P. Luz, V.C. Pandolfelli, Nontoxic processing of reliable macro-porous ceramics, *Int. J. Appl. Ceram. Technol.* 13 (2016) 522–531. doi:10.1111/ijac.12521.
- [24] R. Salomão, V.L. Ferreira, I.R. de Oliveira, A.D.V. Souza, W.R. Correr, Mechanism of pore generation in calcium hexaluminate (CA₆) ceramics formed *in situ* from calcined alumina and calcium carbonate aggregates, *J. Eur. Ceram. Soc.* 36 (2016) 4225–4235. doi:10.1016/j.jeurceramsoc.2016.05.026.
- [25] ASTM, E1875-13: Standard test method for dynamic Young's modulus, shear modulus, and Poisson's ratio by sonic resonance, (2013). doi:10.1520/E1875-13.
- [26] ASTM, C133—97: Standard test methods for cold crushing strength and modulus of rupture of refractories, (2015). doi:10.1520/C0133-97R15.
- [27] C. Felipe Linares, P. Bretto, R. Álvarez, F. Ocanto, C. Corao, P. Betancourt, J.L. Brito, Evaluation of calcined hydrocalumite-type materials as supports of CoMo and NiMo for thiophene hydrodesulfuration reaction, *Mater. Res.* 17 (2014) 823–828. doi:10.1590/S1516-14392014005000085.
- [28] A. Irabien, A. Toquero, M.I. Ortiz, Kinetic behaviour of non-isothermal lime hydration, *Chem. Eng. J.* 40 (1989) 93–99. doi:10.1016/0300-9467(89)80050-4.
- [29] Y. Wang, X. Li, B. Zhu, P. Chen, Microstructure evolution during the heating process and its effect on the elastic properties of CAC-bonded alumina castables, *Ceram. Int.* 42 (2016) 11355–11362. doi:10.1016/j.ceramint.2016.04.058.
- [30] F.A. Cardoso, M.D.M. Innocentini, M.F.S. Miranda, F.A.O. Valenzuela, V.C. Pandolfelli, Drying behavior of hydratable alumina-bonded refractory castables, *J. Eur. Ceram. Soc.* 24 (2004) 797–802. doi:10.1016/S0955-2219(03)00326-1.
- [31] S.R. Klaus, J. Neubauer, F. Goetz-Neunhoeffler, Hydration kinetics of CA₂ and CA—Investigations performed on a synthetic calcium aluminate cement, *Cem. Concr. Res.* 43 (2013) 62–69. doi:10.1016/j.cemconres.2012.09.005.
- [32] F.A. Cardoso, M.D.M. Innocentini, M.M. Akiyoshi, V.C. Pandolfelli, Effect of curing time on the properties of CAC bonded refractory castables, *J. Eur. Ceram. Soc.* 24 (2004) 2073–2078. doi:10.1016/S0955-2219(03)00371-6.
- [33] I.R. Oliveira, F.S. Ortega, V.C. Pandolfelli, Hydration of CAC cement in a castable refractory matrix containing processing additives, *Ceram. Int.* 35 (2009) 1545–1552. doi:10.1016/j.ceramint.2008.08.014.
- [34] A.P. Luz, V.C. Pandolfelli, Halting the calcium aluminate cement hydration process, *Ceram. Int.* 37 (2011) 3789–3793. doi:10.1016/j.ceramint.2011.06.034.
- [35] H.U. Rammelberg, T. Schmidt, W. Ruck, Hydration and dehydration of salt hydrates and hydroxides for thermal energy storage - kinetics and energy release, *Energy Procedia.* 30 (2012) 362–369. doi:10.1016/j.egypro.2012.11.043.
- [36] A.L. Pereira, M.A. Reis, L.L.H.C. Ferreira, E.R. Passos, L.C. Ribeiro, M.M.M. Novo, P.M. Nakachima, Characterization of a new sintered calcium aluminate cement, *Refract. Worldforum.* 3 (2017) 3–6.

Figure Captions

Figure 1: Elastic modulus evolution in alumina based castables as a function of temperature and the Ca^{2+} source [14].

Figure 2: Infrared spectra of (a) CL370, CaCO_3 and (b) CL370, $\text{Ca}(\text{OH})_2$ and the samples produced by combining these raw materials following the steps described in Section 2.1. Both figures show the infrared spectra of hydrocalumite as reported in the literature [17].

Figure 3: X-ray diffraction patterns of compositions containing alumina and CaCO_3 or $\text{Ca}(\text{OH})_2$ after thermal treatment at $700\text{ }^\circ\text{C}$ for 5 hours.

Figure 4: *In situ* elastic modulus as a function of temperature for alumina-based foams with different CaCO_3 content.

Figure 5: Crushing strength and linear shrinkage of 2.04 % CaCO_3 +CAC samples fired at different temperatures. Green samples presented cold crushing strength of (0.51 ± 0.04) MPa and total porosity of (83 ± 2) %.

Figure 6: *In situ* elastic modulus as a function of temperature for alumina-based ceramic foams with different Ca^{2+} sources.

Figure 7: X-ray diffraction patterns of alumina-based ceramic foams fired at $1600\text{ }^\circ\text{C}$ for 5 hours. Number 1 represents corindum and number 2 is for hibonite (CA_6).

Figures

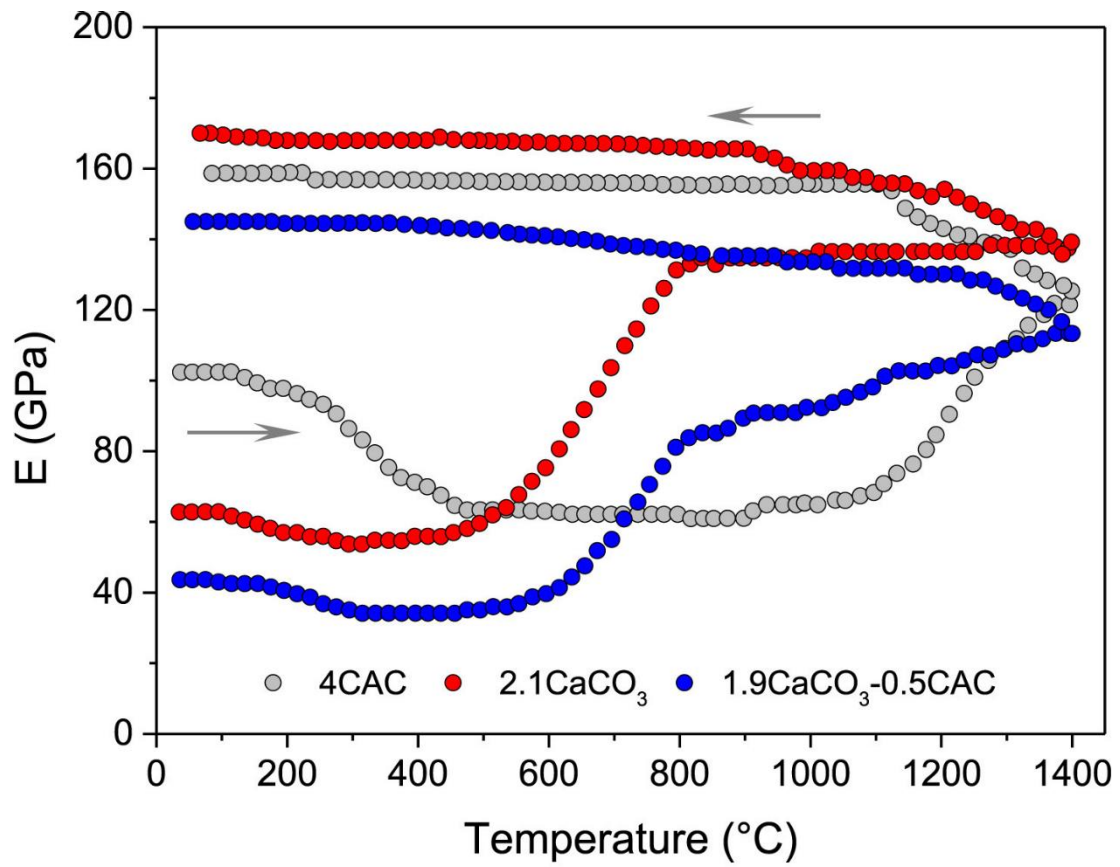


Figure 1: Elastic modulus evolution in alumina based castables as a function of temperature and the Ca²⁺ source [14].

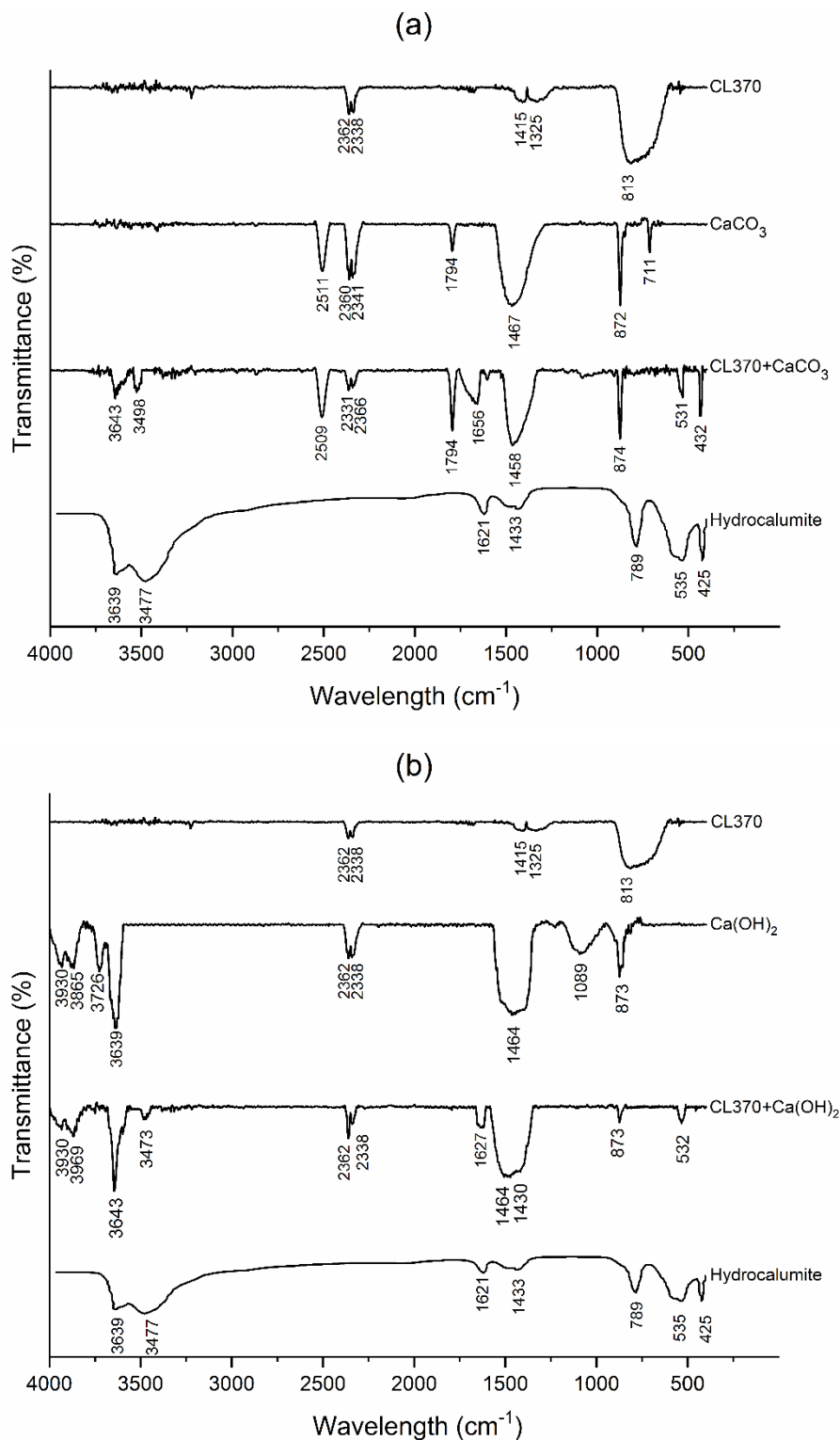


Figure 2: Infrared spectra of (a) CL370, CaCO_3 and (b) CL370, Ca(OH)_2 and the samples produced by combining these raw materials following the steps described in Section 2.1. Both figures show the infrared spectra of hydrocalumite as reported in the literature [17].

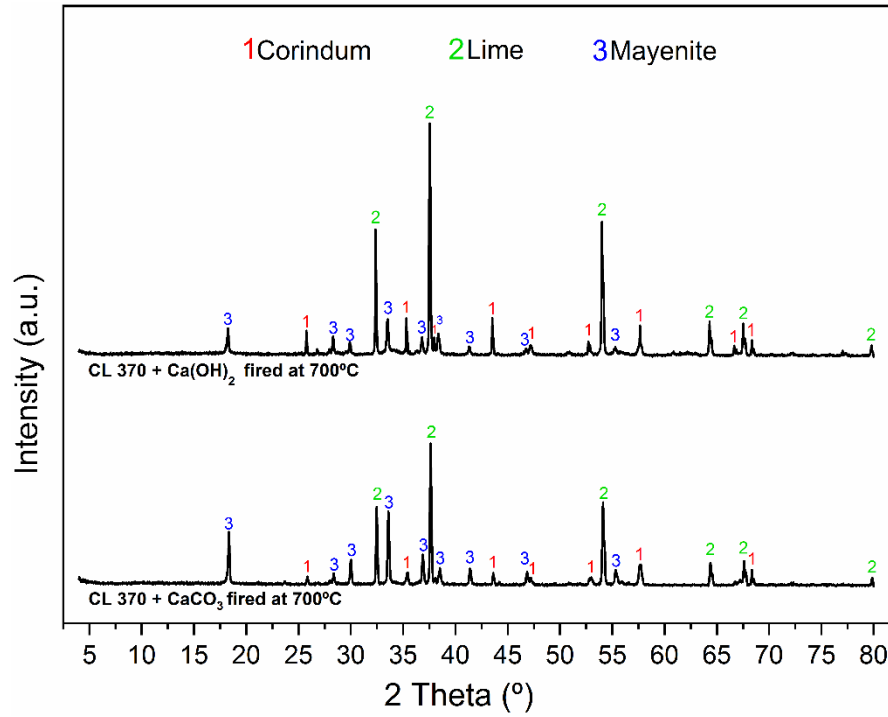


Figure 3: X-ray diffraction patterns of compositions containing alumina and CaCO₃ or Ca(OH)₂ after thermal treatment at 700 °C for 5 hours.

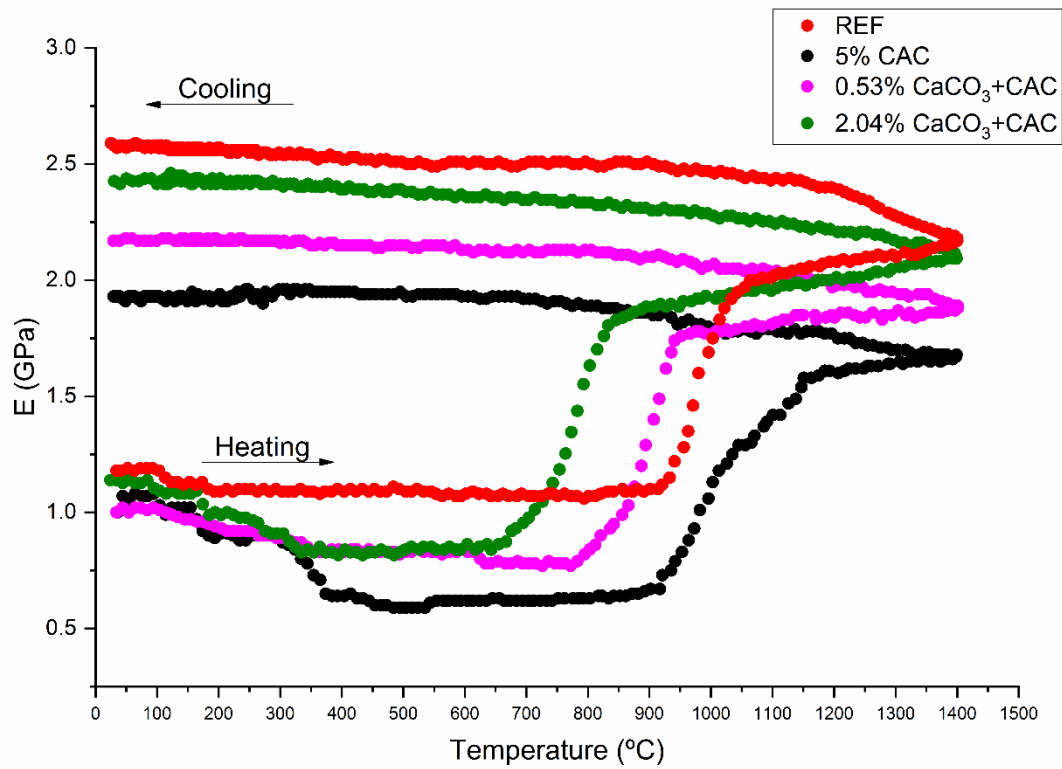


Figure 4: *In situ* elastic modulus as a function of temperature for alumina-based foams with different CaCO₃ content.

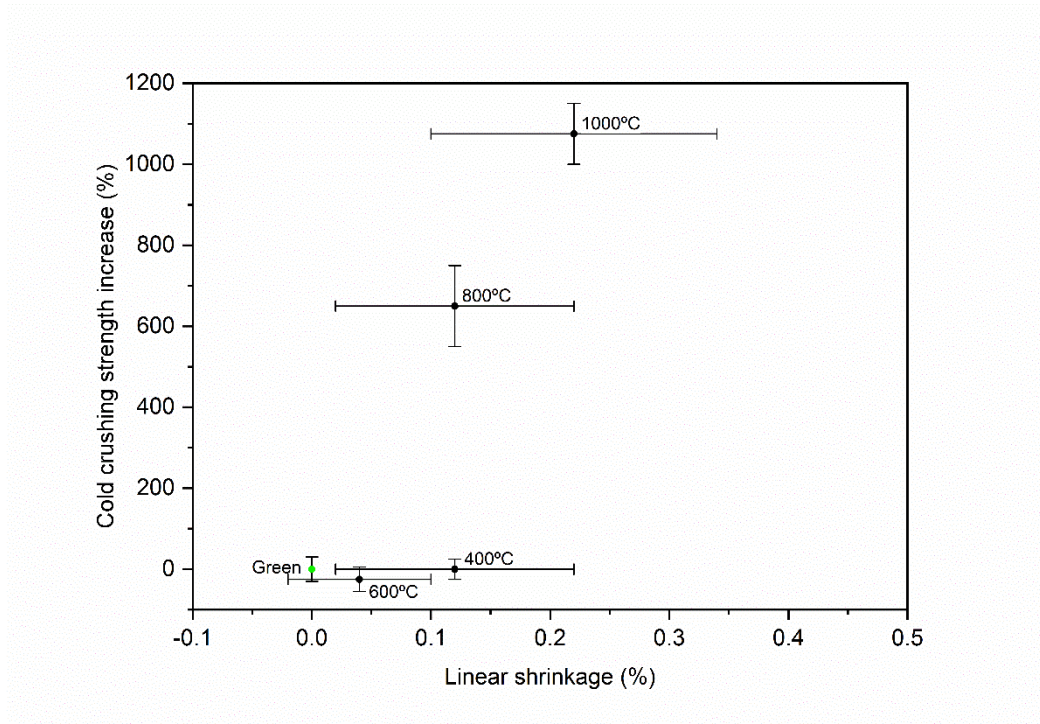


Figure 5: Crushing strength and linear shrinkage of 2.04 % CaCO_3 +CAC samples fired at different temperatures. Green samples presented cold crushing strength of (0.51 ± 0.04) MPa and total porosity of (83 ± 2) %.

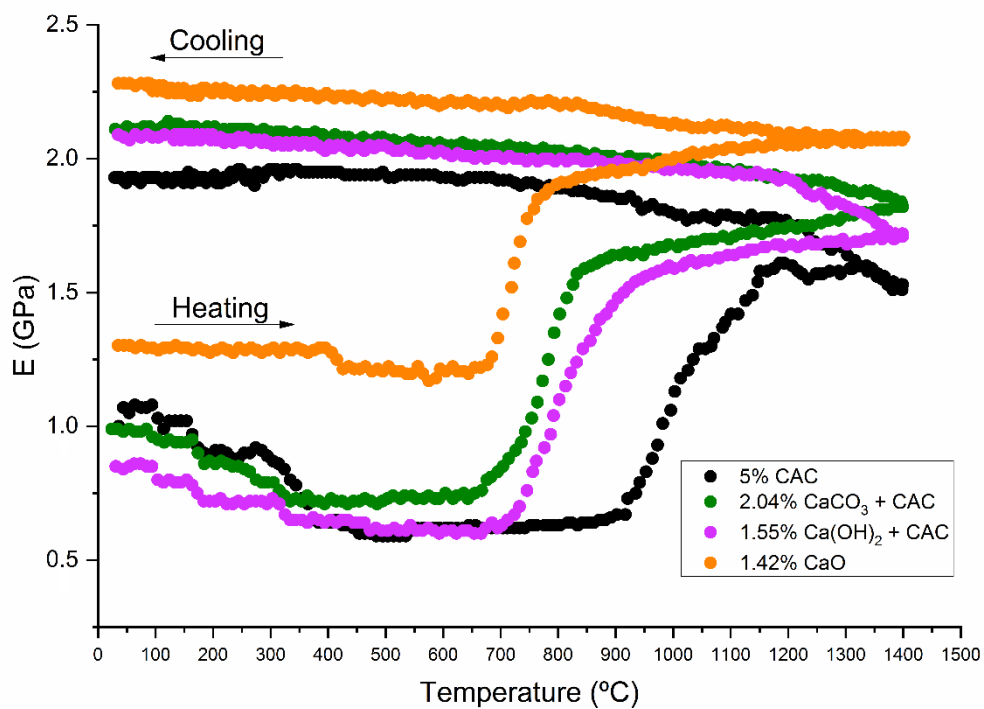


Figure 6: *In situ* elastic modulus as a function of temperature for alumina-based ceramic foams with different Ca^{2+} sources.

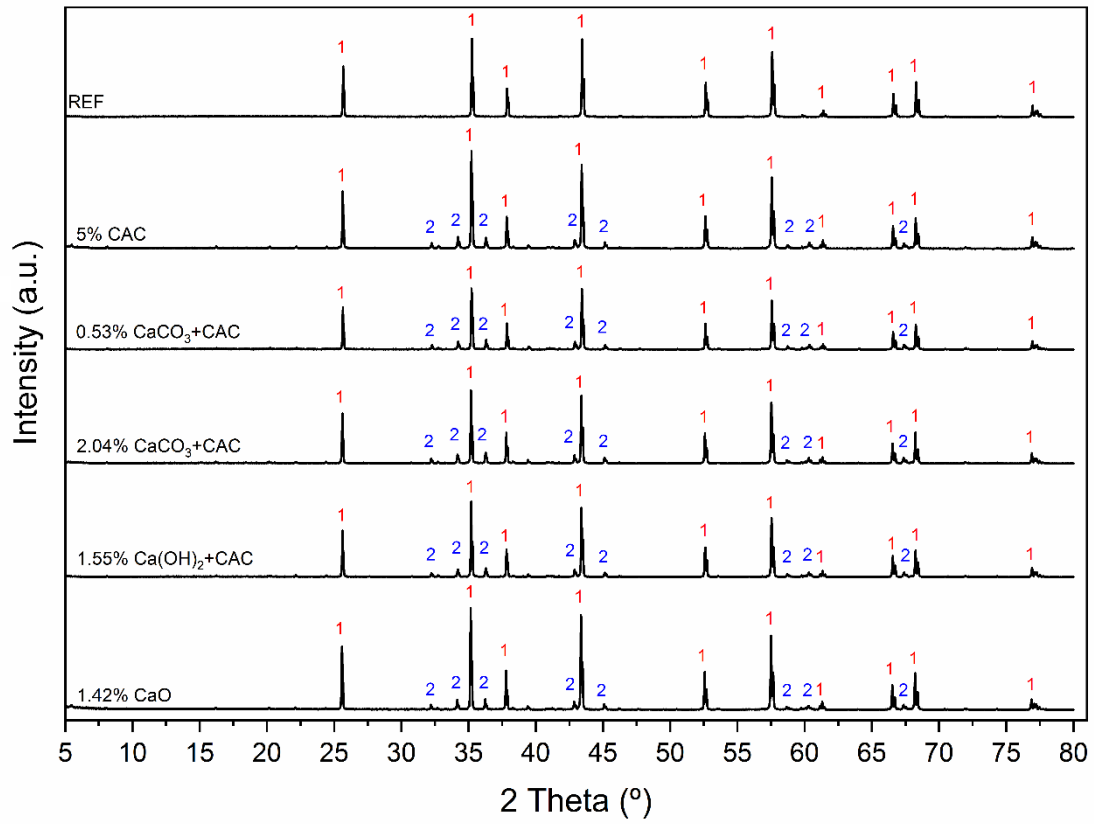


Figure 7: X-ray diffraction patterns of alumina-based ceramic foams fired at 1600 °C for 5 hours. Number 1 represents corundum and number 2 is for hibonite (CA₆).